

Probing high-energy and band-edge exciton dynamics in monolayer WS_2 using transient absorption spectroscopy under near-resonant and high-energy excitations

Hang Ren(任航), Shuai Zhu(朱帅), Mingzhao Ouyang(欧阳名钊), Jiake Wang(王加科), Yuegang Fu(付跃刚), Chuxin Yan(闫楚欣), Qingbin Wang(王庆彬), and Yuanzheng Li(李远征)

Citatio: Chin. Phys. B, 2025, 34 (**9**): 097104. DOI: 10.1088/1674-1056/adf61d
http://cpb.iphy.ac.cn; http://iopscience.iop.org/cpb

What follows is a list of articles you may be interested in

Valley-selective manipulation of moiré excitons through optical Stark effect

Chenran Xu(徐晨燃), Jichen Zhou(周纪晨), Zhexu Shan(单哲旭), Wenjian Su(苏文健), Kenji Watanabe, Takashi Taniguchi, Dawei Wang(王大伟), and Yanhao Tang(汤衍浩)

Chin. Phys. B, 2025, 34 (**1**): 017102. DOI: 10.1088/1674-1056/ad7c32

Excitonic optical properties in monolayer SnP_2S_6

Peng-Yuan Chen(陈鹏远), Zhen Quan(权真), and Shu-Dong Wang(王舒东)

Chin. Phys. B, 2024, 33 (**10**): 107105. DOI: 10.1088/1674-1056/ad73b5

Strain tunable excitonic optical properties in monolayer Ga_2O_3

Hao-Lei Cui(崔浩磊), Zhen Quan(权真), and Shu-Dong Wang(王舒东)

Chin. Phys. B, 2024, 33 (**10**): 107104. DOI: 10.1088/1674-1056/ad74e7

Exciton dynamics in different aromatic hydrocarbon systems

Milica Rutonjski†, Petar Mali, Slobodan Rado\v sevi\'c, Sonja Gombar, Milan Panti\'c, and Milica Pavkov-Hrvojevi\'c

Chin. Phys. B, 2020, 29 (**10**): 107103. DOI: 10.1088/1674-1056/aba2de

Tuning electronic properties of the S_2/graphene heterojunction by strains from density functional theory

Jun-Hui Lei(雷军辉), Xiu-Fen Wang(王秀峰), Jian-Guo Lin(林建国)

Chin. Phys. B, 2017, 26 (**12**): 127101. DOI: 10.1088/1674-1056/26/12/127101

SPECIAL TOPIC — Exciton physics: Fundamentals, materials and devices

Probing high-energy and band-edge exciton dynamics in monolayer WS_2 using transient absorption spectroscopy under near-resonant and high-energy excitations

Hang Ren(任航)[1], Shuai Zhu(朱帅)[1], Mingzhao Ouyang(欧阳名钊)[1], Jiake Wang(王加科)[1], Yuegang Fu(付跃刚)[1], Chuxin Yan(闫楚欣)[2], Qingbin Wang(王庆彬)[2], and Yuanzheng Li(李远征)[2,†]

[1] *School of Optoelectronic Engineering, Changchun University of Science and Technology, Changchun* 130022, *China*

[2] *State Key Laboratory of Integrated Optoelectronics, and Key Laboratory of UV-Emitting Materials and Technology of Ministry of Education, Northeast Normal University, Changchun* 130024, *China*

(Received 23 June 2025; revised manuscript received 21 July 2025; accepted manuscript online 31 July 2025)

Insight into exciton dynamics of two-dimensional (2D) transition metal dichalcogenides (TMDs) is critical for the optimization of their performance in photonic and optoelectronic devices. Although current researches have primarily concentrated on the near-resonant excitation scenario in 2D TMDs, the case of excitation energies resonating with high-energy excitons or higher energies has yet to be fully elucidated. Here, a comparative analysis is conducted between high-energy excitation (360 nm) and near-resonant excitation (515 nm) utilizing transient absorption spectroscopy to achieve a comprehensive understanding of the exciton dynamics within monolayer WS_2. It is observed that the high-energy C-exciton can be generated via an up-conversion process under 515 nm excitation, even the energy of which is less than that of the C-exciton. Furthermore, the capacity to efficiently occupy band-edge A-exciton states leads to longer lifetimes for both the C-excitons and the A-excitons under conditions of near-resonant excitation, accompanied by an augmented rate of radiative recombination. This study provides a paradigm for optimizing the performance of 2D TMDs-based devices by offering valuable insights into their exciton dynamics.

Keywords: monolayer WS_2, C-exciton, A-exciton, exciton dynamics, transient absorption spectroscopy

PACS: 71.35.–y, 71.35.Cc, 78.47.–p, 78.47.jb, 78.55.–m

DOI: 10.1088/1674-1056/adf61d **CSTR:** 32038.14.CPB.adf61d

1. Introduction

Two-dimensional (2D) transition metal dichalcogenides (TMDs) with reduced dielectric screening and enhanced quantum confinement permit a considerable enhancement of the Coulomb interaction experienced by carriers, resulting in the formation of tightly bound excitons and the emergence of complex many-body effects.[1–6] This enables robust light-matter coupling and novel excitonic phenomena, which make TMDs garner considerable research interest, particularly with regard to the advancement of next-generation valleytronic and optoelectronic devices.[7–13] A comprehensive understanding of exciton dynamics, a significant area of research within the broader field of exciton photophysics, is of paramount importance for ensuring the optimal functionality of photonic and optoelectronic devices.

Besides band-edge excitons (i.e., A and B excitons), high-energy excitons have been observed in the 2D TMDs, such as C-excitons, which arise from intrinsic van Hove singularities in the density of states.[14–17] Accordingly, the conduction and valence bands exhibit close parallelism within the Brillouin zone, as shown in Fig. 1(a). Taking WS_2 as an example, the energy difference between the conduction and valence bands is significantly greater than that observed for band-edge excitons, thus demonstrating a high capacity for ultraviolet light absorption, even in a monolayer system (Fig. 1(b)). However, the photoluminescence quantum yield (PLQY) of monolayer TMDs is significantly suppressed at the excitation energies that resonate with high-energy C-excitons or higher energies.[18–20] Previous studies have generally attributed it to the process that only a minor proportion of the high-energy C-excitons are able to evade the unfavorable recombination processes following spontaneous charge separation within a few hundred femtoseconds due to the parallel band structure, subsequently relaxing towards the band edge.[21,22] This results in the formation of limited optically active band-edge excitons that can undergo radiative transitions (Fig. 1(c)) when excitation energies resonate with high-energy C-excitons or higher energies, accompanied by a relatively low PLQY (Fig. 1(d)). Therefore, gaining insight into exciton dynamics at the high excitation energies, particularly in the comparison between near-resonant and high-energy excitations, is essential to efficiently utilize high-energy excitons. While significant progress has been made in understanding exciton dynamics in 2D TMDs, research has primarily focused on the near-resonant excitation scenario,[23–32] leaving a knowledge scarcity regarding the case of excitation energies that resonate with high-energy excitons or higher energies.

†Corresponding author. E-mail: liyz264@nenu.edu.cn

© 2025 Chinese Physical Society and IOP Publishing Ltd. All rights, including for text and data mining, AI training, and similar technologies, are reserved.

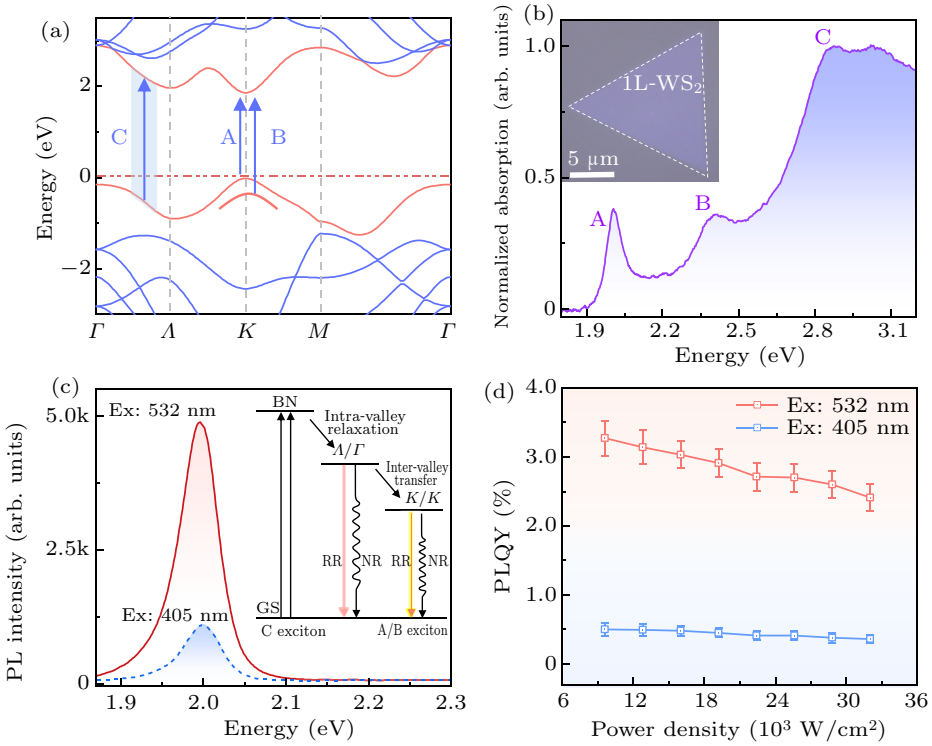


Fig. 1. (a) Theoretically calculated band structure and (b) steady-state absorption spectrum of monolayer WS_2. Inset of (b) is optical microscope image of monolayer WS_2. (c) PL spectra of monolayer WS_2 under 532 nm and 405 nm laser excitation with same output power. (d) Excitation-power-dependent PLQY of CVD-grown monolayer WS_2 under 532 nm and 405 nm laser excitation.

In this study, we conducted a comprehensive comparison of the exciton dynamics in monolayer WS_2 under near-resonant and high-energy excitation conditions utilizing transient absorption (TA) spectroscopy. It was found that under conditions of band-edge B-exciton resonance excitation (515 nm), the C-exciton bleaching signals as those excited at high-energy excitations (360 nm) could be observed. Such a phenomenon can be attributed to the up-conversion process, which enables the generation of C-excitons with higher energy at the B-exciton resonance excitation. Moreover, the more efficient relaxation of photogenerated carriers to the band edge results in extended exciton lifetimes, including the band-edge A-excitons and the high-energy C-excitons, as observed with excitation at 515 nm in comparison to excitation at 360 nm. The results may provide insight into the dynamics and photophysics of excitons in 2D TMDs materials and beyond.

2. Results and discussion

Figure 2(a) shows the photophysical processes of the photocarriers in monolayer WS_2 under near-resonant and high-energy excitation conditions. Herein, the excitation light source of 515 nm resonates with the band-edge B-exciton, whereas the photon energy of the 360 nm light is higher than that of the high-energy C-exciton. Upon exposure to 360 nm, the photogenerated electrons and holes from high-energy C-excitons will undergo further relaxation to the lowest excited state, namely, the band edge at the *K* point, via valley transfer due to parallel band structure. In contrast, excitation at wavelengths of 515 nm results in the generation of photocarriers that can rapidly relax to the band edge through intra-band relaxation processes. It is evident that there are notable distinctions in the dynamics of A-excitons between near-resonant excitation and high-energy excitation, which should be sufficiently elucidated. To this regard, we employed TA spectroscopy to elucidate the A-exciton dynamics under near-resonant and high-energy excitation conditions, utilizing 515 nm and 360 nm as the pump light sources, respectively. Figures 2(b) and 2(c) illustrate representative TA mapping and spectra of a WS_2 monolayer synthesized by chemical vapor deposition (CVD) method when exposed to 360 nm excitation, respectively, with a pump fluence of approximately 5.1 $\mu J \cdot cm^{-2}$. Three distinct photobleaching signals are observed at approximately 610 nm (2.03 eV), 515 nm (2.41 eV), and 432 nm (2.87 eV), respectively. They are attributed to the A, B, and C excitons, respectively, as illustrated in the steady-state absorption spectrum in Fig. 1(b). When exposed to the 515 nm light, the photobleaching signal of the B-exciton overlaps with the pump light to such an extent that it cannot be observed. Intriguingly, the bleaching signal is observed not only for the A-exciton, but also for the peak at the anomalous position of the C-exciton at $\sim$ 432 nm, as shown in Figs. 2(d) and 2(e). It is important to note that the energy of the pump light at 515 nm is less than that of the C exciton. Consequently, direct excitation to produce the C-excitons cannot be accomplished with this light source alone.

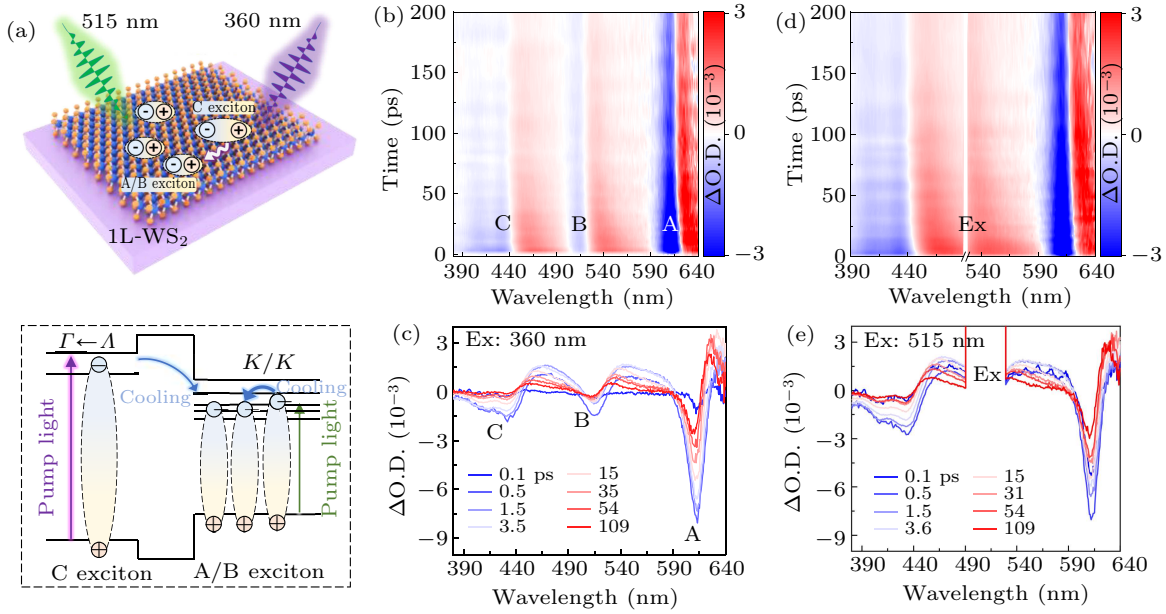


Fig. 2. (a) Schematic of the photophysical processes of the photocarriers in monolayer WS_2 under near-resonant (515 nm) and high-energy (360 nm) excitation conditions. (b) Spectrally and temporally resolved transient absorption map with a pump beam of 360 nm and a pump fluence of 5.1 μJ·cm^{-2}. (c) TA spectra of monolayer WS_2 probed at different delay times extracted from (b). (d) Spectrally and temporally resolved transient absorption map with a pump beam of 515 nm and a pump fluence of 5.1 μJ·cm^{-2}. (e) TA spectra of monolayer WS_2 probed at different delay times extracted from (d).

To clarify the origin of this bleaching peak, we have conducted TA spectra with varying pump fluences and delay times under 515 nm and 360 nm excitation, respectively. Figure 3(a) illustrates the TA spectra within the wavelength range of 380–510 nm at a delay time of 0.5 ps under pump wavelengths of 515 nm and 360 nm, respectively, as pump fluences increase from 1 μJ·cm^{-2} to 5.1 μJ·cm^{-2}. It can be observed that the peak position at ∼ 432 nm remains almost unchanged with an increase in pump fluence when exposed to 515 nm excitation, and meanwhile the peak positions demonstrate consistency when compared to the results observed at 360 nm excitation. Obviously, neither the band renormalization effect nor the band-filling effect is applicable to the C-exciton states within the specified low pump fluence range.[33–36] Moreover, the transient bleaching peaks exhibit comparable independence in delay time and analogous positions for both the 515 nm and 360 nm excitation wavelengths, as plotted in Fig. 3(b). The similarity in peak position and its independence on pump fluence and delay time provide sufficient evidence to conclude that the bleaching peak at ∼ 432 nm under 515 nm excitation can be attributed to the C-exciton states. This signifies the necessity for the generation of high-energy C-excitons via an up-conversion process when exposed to 515 nm pump light, the energy of which is less than that of the C-exciton.

To validate the existence of the up-conversion process, a comparison was conducted between the rising time of the C-exciton dynamic curve under 515 nm and 360 nm excitation. As illustrated in Fig. 3(c), the C-exciton dynamic curve demonstrates a relatively slower rise under 515 nm excitation in comparison to that under 360 nm excitation, with a difference in rising time of up to ∼ 80 fs. The result can be attributed to the increase in the formation time of the C-exciton, as the up-conversion processes involving multiple steps result in an extension of the timescale associated with the filling of the C-exciton states. It is crucial to acknowledge that both two-photon absorption and Auger recombination are capable of achieving up-conversion process.[37] With regard to two-photon absorption, it is capable of producing a photogenerated electron–hole pair with energy that is twice that of the incident photon. This indicates that as the energy of the incident photon increases, the cooling process of the photogenerated carriers to the C-exciton states is prolonged. Consequently, the rising time of the C-exciton dynamic curve is proportional to the incident photon energy in the case of two-photon absorption. In contrast, the Auger recombination of A-excitons contributes to the C-excitons, with the transfer of energy from one A-exciton enabling the other to be excited to the C-exciton states.[38,39] In other words, this process entails the interaction of two A-excitons, which fuse together to form a high-energy C-exciton. It can be observed that the Auger rate is generally less dependent on the energy of the incident photon. To this regard, we have selected 480 nm, 507 nm, and 608 nm as pump light sources for probing the C-exciton dynamics via the up-conversion process, as illustrated in Fig. S1. Here, the peak at ∼ 432 nm persists across all three excitation sources, consistent with C-exciton ground-state bleaching signals. The corresponding rising processes of the C-exciton dynamic curves, excited by the three pump beams, have been extracted and are presented in Fig. 3(d). In comparison with 360 nm excitation, the three dynamic curves of C-excitons demonstrate a longer rising time, with corresponding differences in rising time of approximately 90 fs, 70 fs, and 85 fs, respectively (see

Fig. 3(e)). These remain on an analogous timescale to the difference in rise time under 515 nm excitation. It follows that the rising time of the C-excitons is largely independent of the incident photon energy, and the Auger recombination of band-edge A-excitons is the primary mechanism governing the up-conversion process.

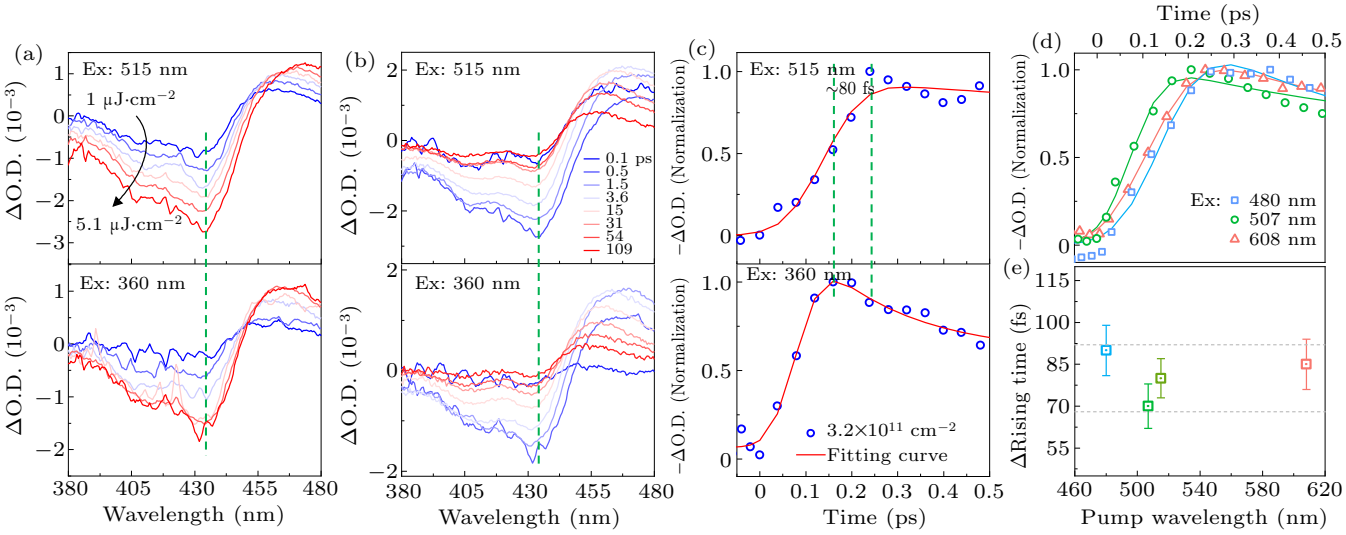


Fig. 3. (a) Pump fluence-dependent TA spectra of C-exciton under pump wavelengths of 515 nm (top panel) and 360 nm (bottom panel) at a delay time of 0.5 ps, where the pump fluences increase from 1 μJ·cm^{-2} to 5.1 μJ·cm^{-2}. (b) Delay time-dependent TA spectra of C-exciton under 515 nm (top panel) and 360 nm pump (bottom panel) with a pump fluence of 5.1 μJ·cm^{-2}. (c) Comparison of normalized decay dynamics of C-exciton of monolayer WS_2 within the first several tenths of a picosecond between 515 nm (top panel) and 360 nm (bottom panel) excitation. (d) Normalized decay dynamics of C-exciton of monolayer WS_2 within the first several tenths of a picosecond under 480 nm, 507 nm and 608 nm excitation. (e) The rising time of C-exciton dynamics as a function of pump wavelengths.

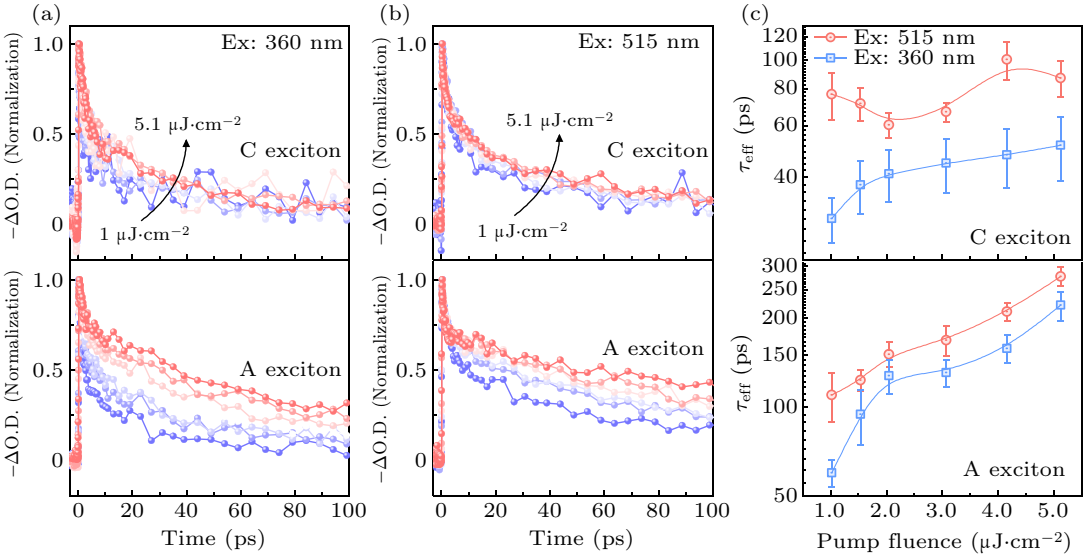


Fig. 4. Pump fluence-dependent decay dynamics of C- (top panel) and A-exciton (bottom panel) under (a) 360 nm and (b) 515 nm excitation from 1 μJ cm^{-2} to 5.1 μJ cm^{-2}. (c) The effective lifetime (τ_{eff}) of C- (top panel) and A-exciton (bottom panel) as a function of pump fluences under 360 nm and 515 nm excitation, respectively.

To gain further insight into the exciton dynamics under conditions of near-resonant excitation and high-energy excitation, we have conducted pump fluence-dependent TA measurements, performed with excitation wavelengths of 360 nm and 515 nm, respectively. Figures 4(a) and 4(b) show the pump fluence-dependent C- and A-exciton dynamic curves under 360 nm and 515 nm excitation, respectively. The pump fluence was increased from 1 μJ cm^{-2} to 5.1 μJ·cm^{-2}, at which point the excitation density at both pump beams was maintained at a similar order of magnitude (10^{11}–10^{12} cm^{-2}). The A-exciton and C-exciton decay curves exhibit comparable dynamic behaviors under 360 nm and 515 nm excitation, respectively. That is, the C-exciton decay exhibits a relatively weak pump fluence dependence, while the A-exciton decay demonstrates a considerably stronger dependence on the pump fluence. Figure 4(c) demonstrates the quantitative fitting of the decay curves of C- and A-excitons, which were measured at both pump beams with varying pump fluences. The decay curves were also fitted using a tri-exponential function of the form $A_1\exp(-t/\tau_1)+A_2\exp(-t/\tau_2)+A_3\exp(-t/\tau_3)$,

where A_1, A_2 and A_3 represent the weight factors, and τ_1, τ_2 and τ_3 denote the time constants. For the A-exciton, as previously reported,[40] the three components correspond to surface-defect trapping, carrier-phonon scattering, and direct electron–hole recombination. In the case of the C-exciton, the components may be assigned to intervalley transfer, with distinct rates arising from different phonon-mediated scattering pathways.[41] Here, the effective lifetime (τ_{eff}) is used as a descriptive measure of exciton lifetime for convenience. More details are available in supporting information Figs. S2–S5 and Table S1. Intriguingly, the τ_{eff} of C- and A-excitons under 515 nm excitation are observed to be greater than those observed under 360 nm excitation, respectively. With regard to the C-excitons, the τ_{eff} demonstrate a comparatively weaker dependence on pump fluence under excitation at 515 nm, while exhibiting a slight increase from 30 ps to 51 ps with elevated pump fluence under 360 nm excitation. For the A-excitons, it was observed that the τ_{eff} increased markedly with an enhancement in pump fluence under excitation at both pump beams. In general, the lifetimes of excitons with increasing pump fluences are either unchanged or diminished due to an increase in many-body processes such as Auger recombination and exciton–exciton annihilation (EEA).[42–45]

To interpret the discrepancy in the exciton lifetime in comparison to that of near-resonant and high-energy excitation, as well as the relationship between pump fluence and lifetime, it is first necessary to elucidate the physical processes occurring in photocarriers under down-conversion and up-conversion conditions, as illustrated in Fig. 5. In the down-conversion process, the parallel band structure allows photocarriers from C-excitons (electrons and holes) to relax rapidly within a sub-picosecond timescale to the Λ valley/Γ hill, respectively. Subsequently, they transfer to the band-edge state (K valley/hill) via intervalley transfer with a timescale of tens of picoseconds. During the aforementioned process, however, only a few hot carriers are capable of evading the unfavorable recombination processes and relaxing towards the band edges. That results in the formation of a limited number of occupied states from A-excitons, leading to a PLQY that is relatively low (Fig. 1(d)). In contrast, the photocarriers (electrons and holes) can rapidly cool to the K valley/hill within a sub-picosecond timescale via intra-valley relaxation under near-resonant excitation, with the formation of only a few unoccupied A-exciton states. Simultaneously, the band edge A-excitons could effectively generate the C-excitons via the up-conversion process, and then the hot carriers from C-excitons exhibit the same relaxation pathway as those under conditions of high-energy excitation. It should be noted that upon the effective occupation of the band-edge exciton states, there is no remaining excess of unoccupied energy states for C-exciton cooling. In other words, the relaxation channel of the C-exciton will become blocked, which is known as the Pauli blocking effect, accompanied by an increase in the exciton lifetime.[41] The observed result that the τ_{eff} of C-exciton is greater under 515 nm excitation than under 360 nm excitation demonstrates that band-edge exciton states can be effectively occupied under near-resonant excitation. The τ_{eff} of C-excitons exhibit a slight increase with elevated pump fluence under 360 nm excitation, indicating that the band-edge exciton states at higher power excitation are more effectively occupied. This impedes the relaxation of the C-exciton even under the condition of high-energy excitation. Therefore, the extended lifetime of the C-exciton means a greater population of carriers occupying the C-exciton state. Note that the lifetime of the C-exciton is not capable of continuing to increase, due to the limitations imposed by intervalley scattering rates for carriers.[46,47] It can thus be concluded that the τ_{eff} of the C-exciton attains a saturation value at 515 nm excitation, with a relatively weak dependence on the pump fluence (top panel of Fig. 4(c)). When hot carriers are transferred from the C-exciton to the K valley/hill, they may offset the loss of A-excitons populated at band-edge state and decelerate the decay of A-excitons. This results in the observed lifetime of A-excitons that demonstrates an upward trend with increasing pump fluence levels (bottom panel of Fig. 4(c)). To sum up, the discrepancy between the lifetimes of A-excitons at near-resonant and high-energy excitations can be ascribed to the capacity of band-edge exciton states to be efficiently occupied. In the case of near-resonant excitation, it has been established that A-excitons can not only be effectively filled, but also exhibit a prolonged lifetime and an augmented radiative recombination rate in comparison with high-energy excitation.

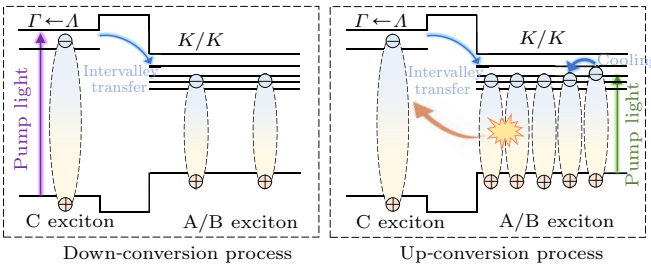


Fig. 5. The physical processes occurring in photocarriers under down-conversion and up-conversion conditions in monolayer WS_2.

3. Conclusion

In summary, a detailed analysis was conducted to compare the exciton dynamics in a monolayer WS_2 under near-resonant (515 nm) and high-energy (360 nm) excitation conditions based on TA spectroscopy. When exposed to 515-nm pump light, not only is the photobleaching signal of band-edge A-exciton observable, but also that of the high-energy C-excitons. In comparison with 360 nm excitation, an analogous independence in transient bleaching peak positions of C excitons on pump fluence and delay time can be observed in the

case of 515 nm excitation, accompanied with longer rise time of C excitons, suggesting that the up-conversion process enables the generation of high-energy C excitons at the B-exciton resonance excitation. Moreover, the capacity of band-edge exciton states to be efficiently occupied results in prolonged lifetimes of the band-edge A-excitons and the high-energy C-excitons in the case of near-resonant excitation, accompanied by an augmented radiative recombination rate. Insight into the exciton dynamics of monolayer WS_2 under near-resonant and high-energy excitations not only enriches the understanding of ultrafast photophysical processes in strong quantum-confined systems, but also may provide the necessary impetus for the development of high-performance ultraviolet light-harvesting devices.

Appendix A: Experimental details

The monolayer WS_2 flake was synthesized via chemical vapor deposition (CVD) on sapphire substrates using sulfur and tungsten trioxide powders as precursors. To demonstrate spatial uniformity, the PL mapping across the monolayer WS_2 flake was performed in Fig. S6. Using a 100× objective lens and an Olympus BX51 microscope system, the optical microscopy image of a monolayer WS_2 flake was acquired. UV2600 spectrophotometer system was used to record steady-state absorption spectra. All of the steady state PL spectra at room temperature were measured using a commercially integrated platform that has several continuous-wave lasers (320 nm, 405 nm, 532 nm, and 638 nm). The PLQY values of monolayer WS_2 were employed as absolute measurements relative to Rhodamine 6G (R6G). More details are available in supporting information Note 1. HELIOS Ultrafast Systems were employed to perform femtosecond TA measurements. An optical parametric amplifier (Coherent, OperA Solo) was pumped with 800 nm pulses from a Coherent Astrella regenerative amplifier (80 fs, 1 kHz, 2.5 mJ per pulse) to generate 400 nm excitation pulses. The probe beam, which was a tiny portion of the Astrella's 800 nm output, was fed into a sapphire crystal in the HELIOS to create the time-delayed white light continuum. The ultimate temporal resolution of the TA system was 100 fs. All measurements were performed under ambient conditions.

Acknowledgements

This work was supported by the National Natural Science Foundation of China (Grant Nos. 12474421 and 12104066), the Fund from Education Department of Jilin Province (Grant Nos. JJKH20250473KJ and JJKH20241413KJ), and the Fund from Department of Science and Technology of Jilin Province (Grant No. YDZJ202101ZYTS041).

References

[1] Mak K F, He K, Lee C, Lee G H, Hone J, Heinz T F and Shan J 2013 *Nat. Mater.* **12** 207
[2] Britnell L, Ribeiro R M, Eckmann A, Jalil R, Belle B D, Mishchenko A, Kim Y J, Gorbachev R V, Georgiou T and Morozov S V 2013 *Science* **340** 1311
[3] You Y, Zhang X X, Berkelbach T C, Hybertsen M S, Reichman D R and Heinz T F 2015 *Nat. Phys.* **11** 477
[4] Qiu D Y, Jornada F H D and Louie S G 2015 *Phys. Rev. Lett.* **115** 216805
[5] Li Y, Yan J, Chen J, Yu T, Ren H, Liu X, Liu W, Yang G, Xu C and Bao Q 2021 *Nano Res.* **14** 4274
[6] Huo C, Yun T, Yan X, Liu Z, Zhao X, Xu W, Cui Q, Liu Z and Tian J 2023 *Chin. Phys. B* **32** 067203
[7] Unuchek D, Ciarrocchi A, Avsar A, Sun Z, Watanabe K, Taniguchi T and Kis A 2019 *Nat. Nanotechnol.* **14** 1104
[8] Ye T, Li Y, Li J, Shen H, Ren J, Ning C Z and Li D 2022 *Light Sci. Appl.* **11** 23
[9] Kwak D, Polyushkin D K and Mueller T 2023 *Nat. Commun.* **14** 4264
[10] Cai H, Rasmita A, He R, Zhang Z, Tan Q, Chen D, Wang N, Mu Z, Eng J J H, She Y, Pan N, Wang Q, Dong Z, Wang X, Wang J, Miao Y, Singh R, Qiu C W, Liu X and Gao W 2024 *Nat. Photonics* **18** 842
[11] Ma R, Ren H, Yan C, Li Y, Li J, Xin W, Liu W, Zhao X G, Yang L, Feng S, Xu H, Liu Y and Liu X 2024 *ACS Photonics* **11** 5339
[12] Li J, Zhou Y, Li Y, Yan C, Zhao X G, Xin W, Xie X, Liu W, Xu H and Liu Y 2024 *ACS Photonics* **11** 4578
[13] Li Y, Liu W, Xu H, Chen H, Ren H, Shi J, Du W, Zhang W, Feng Q and Yan J 2020 *Adv. Opt. Mater.* **8** 1901226
[14] Carvalho A, Ribeiro R M and Castro Neto A H 2013 *Phys. Rev. B* **88** 115205
[15] Yan C, Li Y, Li R, Ma R, Li J, Xin W, Liu W, Xu H and Liu Y 2024 *Laser Photonics Rev.* **18** 2400951
[16] Goswami T, Bhatt H, Babu K J, Kaur G, Ghorai N and Ghosh H N 2021 *J. Phys. Chem. Lett.* **12** 6526
[17] Gao Y, Li Y, Liu W, Yan C, Wang Q, Xin W, Xu H and Liu Y 2025 *Chin. Phys. B* **34** 097102
[18] Feng J, Li Y, Li J, Feng Q, Xin W, Liu W, Xu H and Liu Y 2022 *Nano Lett.* **22** 3699
[19] Yan Z, Poh E T, Zhang Z, Chua S T, Wang X, Wu X, Chen Z, Yang J, Xu Q H and Goh K E J 2020 *ACS Nano* **14** 5946
[20] Yan C, Sun B, Li Y, Li R, Wang Q, Gao Y, Xin W, Liu W, Xu H and Liu Y 2025 *Nano Lett.* **25** 9686
[21] Kozawa D, Kumar R, Carvalho A, Amara K K, Zhao W, Wang S, Toh M, Ribeiro R M, Neto A H C and Matsuda K 2014 *Nat. Commun.* **5** 4543
[22] Qu J, Wei Y, Zhao L, Tan R, Li W, Shi H, Zhang Y, Yang J, Gao B and Li X 2024 *ACS Nano* **18** 34322
[23] Mai C, Barrette A, Yu Y, Semenov Y G, Kim K W, Cao L and Gundogdu K 2014 *Nano Lett.* **14** 202
[24] Jin C, Ma E Y, Karni O, Regan E C, Wang F and Heinz T F 2018 *Nat. Nanotechnol.* **13** 994
[25] Li Y, Shi J, Mi Y, Sui X, Xu H and Liu X 2019 *J. Mater. Chem. C* **7** 4304
[26] Wang Y, Nie Z and Wang F 2020 *Light Sci. Appl.* **9** 192
[27] Wang Z, Altmann P, Gadermaier C, Yang Y, Li W, Ghirardini L, Trovatello C, Finazzi M, Duò L, Celebrano M, Long R, Akinwande D, Prezhdo O V, Cerullo G and Dal Conte S 2021 *Nano Lett.* **21** 2165
[28] Yuan L, Zheng B, Zhao Q, Kempt R, Brumme T, Kuc A B, Ma C, Deng S, Pan A and Huang L 2023 *ACS Nano* **17** 15379
[29] Sun C, Zhou H, Sheng T, Li S and Zhu H 2024 *ACS Nano* **18** 931
[30] Sui X, Wang H, Liang C, Zhang Q, Bo H, Wu K, Zhu Z, Gong Y, Yue S, Chen H, Shang Q, Mi Y, Gao P, Zhang Y, Meng S and Liu X 2022 *Nano Lett.* **22** 5651
[31] Wang Z, Sun C, Xu X, Liu Y, Chen Z, Yang Y M and Zhu H 2023 *J. Am. Chem. Soc.* **145** 11227
[32] Zhou H, Sun C, Xin W, Li Y, Chen Y and Zhu H 2022 *Nano Lett.* **22** 2547
[33] Liu X, Zhang Q, Yip J N, Xiong Q and Sum T C 2013 *Nano Lett.* **13** 5336
[34] Li Y, Wu X, Liu W, Xu H and Liu X 2021 *Appl. Phys. Lett.* **119** 051106
[35] Cunningham P D, Hanbicki A T, McCreary K M and Jonker B T 2017 *ACS Nano* **11** 12601
[36] Pogna E A, Marsili M, De F D, Dal C S, Manzoni C, Sangalli D, Yoon D, Lombardo A, Ferrari A C and Marini A 2015 *ACS Nano* **10** 1182

[37] Wu B, Wang A, Fu J, Zhang Y, Yang C, Gong Y, Jiang C, Long M, Zhou G, Yue S, Ma W and Liu X 2023 *Science Advances* **9** eadi9347

[38] Li Y, Shi J, Chen H, Wang R, Mi Y, Zhang C, Du W, Zhang S, Liu Z, Zhang Q, Qiu X, Xu H, Liu W, Liu Y and Liu X 2018 *Nanoscale* **10** 17585

[39] Wang H, Zhang C and Rana F 2014 *Nano Lett.* **15** 339

[40] Shi H, Yan R, Bertolazzi S, Brivio J, Gao B, Kis A, Jena D, Xing H G, and Huang L 2013 *ACS Nano* **7** 1072

[41] Li Y, Shi J, Chen H, Mi Y, Du W, Sui X, Jiang C, Liu W, Xu H and Liu X 2019 *Laser Photonics Rev.* **13** 1800270

[42] Fuchs G, Schiedel C, Hangleiter A, Härle V and Scholz F 1993 *Appl. Phys. Lett.* **62** 396

[43] Cunningham P D, McCreary K M and Jonker B T 2016 *J. Phys. Chem. Lett.* **7** 5242

[44] Sun D, Rao Y, Reider G A, Chen G, You Y, Brézin L, Harutyunyan A R and Heinz T F 2014 *Nano Lett.* **14** 5625

[45] Lee K J, Xin W and Guo C 2020 *Phys. Rev. B* **101** 195407

[46] Zeng H, Dai J, Yao W, Xiao D and Cui X 2012 *Nat. Nanotechnol.* **7** 490

[47] Li M, Bhaumik S, Goh T W, Kumar M S, Yantara N, Grätzel M, Mhaisalkar S, Mathews N and Sum T C 2017 *Nat. Commun.* **8** 14350